Binding of human Cdc123 to eIF2γ

Cristina Cardenal Peralta, Paul Vandroux, Lea Neumann-Arnold, Michel Panvert, Jérôme Fagart, Wolfgang Seufert, Yves Mechulam, Emmanuelle Schmitt

Binding of human Cdc123 to eIF2γ

Cristina Cardenal Peralta[1], Paul Vandroux[1], Lea Neumann-Arnold[2], Michel Panvert[1], Jérôme Fagart[1], Wolfgang Seufert[2], Yves Mechulam[1] and Emmanuelle Schmitt[1]

[1] Laboratoire de Biologie Structurale de la Cellule, BIOC, Ecole polytechnique, CNRS, Institut Polytechnique de Paris, 91128 Palaiseau cedex, France.

[2] Department of Genetics, Regensburg Center for Biochemistry, University of Regensburg, Regensburg, Germany.

*Co-corresponding authors: emmanuelle.schmitt@polytechnique.edu and Wolfgang.Seufert@ur.de

SUMMARY

Eukaryotic initiation factor 2 (eIF2) plays a key role in protein synthesis and in its regulation. The assembly of this heterotrimeric factor is facilitated by Cdc123, a member of the ATP grasp family that binds the γ subunit of eIF2. Notably, some mutations related to MEHMO syndrome, an X-linked intellectual disability, affect Cdc123-mediated eIF2 assembly. The mechanism of action of Cdc123 is unclear and structural information for the human protein is awaited. Here, the crystallographic structure of human Cdc123 (Hs-Cdc123) bound to domain 3 of human eIF2γ (Hs-eIF2γD3) was determined. The structure shows that the domain 3 of eIF2γ is bound to domain 1 of Cdc123. Moreover, the long C-terminal region provides a link between the ATP binding site on Hs-Cdc123 and Hs-eIF2γD3. A thermal shift assay shows that ATP is tightly bound to Cdc123 whereas the affinity of ADP is much smaller. Yeast cell viability experiments, western blot analysis and two-hybrid assays show that ATP is important for the function of Hs-Cdc123 in eIF2 assembly. These data and recent findings allow us to propose a refined model to explain the mechanism of action of Cdc123 in eIF2 assembly.

The heterotrimeric initiation factor 2 (e/aIF2) has a central role in eukaryotic and archaeal translation initiation (Hinnebusch, 2014; Schmitt et al., 2020). It is composed of three subunits α, β, γ. The γ subunit forms the core of the heterotrimer and binds GTP. α and β subunits are bound to γ but do not interact with each other (Schmitt et al., 2010). In canonical eukaryotic translation initiation, eIF2:GTP specifically binds the methionyl-initiator tRNA and carries it to the small ribosomal subunit to form, in the presence of other initiation factors, a pre-initiation complex (PIC) able to scan the mRNA to search for a start codon in a correct nucleotidic context. Once the start codon has been found, eIF2 is released from the PIC in its GDP-bound form. Final steps of translation initiation allow the recruitment of the large ribosomal subunit and the formation of a ribosome competent for elongation (Kazan et al., 2023). Specific binding of the initiator tRNA to eIF2-GTP and the control of the nucleotide state of the factor are crucial for efficient translation initiation (Dubiez et al., 2015; Hinnebusch, 2014). Once eIF2-GDP is released from the PIC, the guanine nucleotide exchange factor eIF2B catalyzes recycling of eIF2-GDP to eIF2-GTP to allow additional rounds of translation initiation (Pavitt, 2018). However, stress conditions, such as amino acid deprivation, viral infection or increase of the load of unfolded proteins in the endoplasmic reticulum, trigger phosphorylation of the α subunit of eIF2 at the Serine 52 residue (S51 in yeast) by eIF2α-specific kinases (Wek, 2018). Phosphorylated eIF2α tightly binds eIF2B and prevents its recycling activity (Krishnamoorthy et al., 2001). As a consequence, the global availability of eIF2-GTP decreases leading to a global attenuation of protein synthesis. Importantly, translation of some mRNAs (most of them containing short open reading frames upstream from the main one, uORFs) coding for regulatory proteins is activated by the low levels of eIF2:GTP:Met-$tRNA_i^{Met}$ and allows the cell to respond to stress. This specific response called ISR (integrated stress-response) is crucial to recover cellular homeostasis and deregulation of ISR are linked to a wide range of human diseases (Wek, 2018).

In eukaryotes, the assembly of the heterotrimeric protein eIF2 is facilitated by the Cdc123 protein (Perzlmaier et al., 2013). Indeed, Cdc123 interacts with eIF2γ (Bieganowski et al., 2004; Chen et al., 2023; Ho et al., 2002) and the association of eIF2γ to eIF2α and eIF2β was shown to depend on

the interaction of the C-terminal domain (D3) of eIF2γ with Cdc123 in yeast and human (Panvert et al., 2015; Perzlmaier et al., 2013; Vanselow et al., 2022). Moreover, the C-terminal region of *S. cerevisiae* Cdc123 (the last 30 residues) is indispensable for its *in vivo* function (Panvert et al., 2015). In yeast, human and plants, mutations in Cdc123 lower the availability of functional eIF2 and dysregulate protein synthesis triggering ISR (Chen et al., 2023; Perzlmaier et al., 2013; Vanselow et al., 2022; Young-Baird et al., 2020). Notably, mutations related to MEHMO syndrome (Mental deficiency, Epilepsy, Hypogenitalism, Microcephaly and Obesity), an X-linked intellectual disability, were found in the gene encoding eIF2γ in mammals (*EIF2S3*) (Gregory et al., 2019; Kotzaeridou et al., 2020; Moortgat et al., 2016; Skopkova et al., 2017). One mutation (eIF2γ-I222T) impairs the binding of eIF2β to eIF2γ (Borck et al., 2012). Another impairs the binding of the initiator tRNA to eIF2 (eIF2γ-I259M) (Young-Baird et al., 2019). Some other mutations are located close to the GTP binding site in eIF2γ domain 1 (Kotzaeridou et al., 2020). The P432S mutation, located in the domain 3 of eIF2γ is additionally related to hypopituitarism and glucose dysregulation (Gregory et al., 2019). The mechanism for the pathological effect of this mutation has not been described yet. Finally, a mutation corresponds to a 4-nucleotide deletion near to the 3' end of the EIF2S3 coding region that changes the C-terminal amino acid sequence of eIF2γ from G_{462}VTIKPTVDD to G_{462}VTSQQ (Moortgat et al., 2016). This frameshift mutation (eIF2γ-I465Sfs*4 also abbreviated eIF2γ-fs) impairs the Cdc123-assisted assembly of eIF2 (Young-Baird et al., 2020) but the mechanism remains to be described. Overall, the data suggest that Cdc123-assisted eIF2 assembly can be a new node of translation regulation from yeast to human. Notably, *CDC123* is part of the essential genes in human, which only include about 10% of all human genes (Wang et al., 2015).

The crystallographic structure of *Schizosaccharomyces pombe* Cdc123 (Sp-Cdc123) showed that the protein belongs to the ATP grasp family. Binding of ATP was indeed observed in the structure and Cdc123 variants in the ATP binding pocket suggested that ATP was important for the Cdc123 function (Chen et al., 2023; Panvert et al., 2015; Perzlmaier et al., 2013; Vanselow et al., 2022). On the other hand, the crystallographic structure of Sp-Cdc123 bound to the domain 3 of eIF2γ from S*accharomyces cerevisiae* (Sc-eIF2γD3 or simply Sc-γD3) was determined (Sp-Cdc123:Sc-eIF2γD3).

This structure showed how Sc-eIF2γD3 is bound to domain I of Sp-Cdc123 in yeast. However, the C-terminal tail of Cdc123 was not visible in the structure, leaving the essential function of this region unexplained. A docking of the eIF2αγ structure onto Cdc123, combined with genetic and biochemical experiments, allowed the authors to propose a model for the role of Cdc123 in the assembly of eIF2γ to eIF2α (Panvert et al., 2015). Despite these recent findings based on the structure of a heterologous complex, the mechanism of action of Cdc123 remains unclear and structural information for the human protein is still awaited.

In the present study, we determined the crystallographic structure of human Cdc123 (Hs-Cdc123) bound to human eIF2γD3 (Hs-eIF2γD3) domain. The overall structure of the human complex is similar to that of the yeast complex. However, the present structure shows how the long C-terminal region of Hs-Cdc123 interacts with Hs-eIF2γD3 and is connected to the ATP binding site. We also used a thermal shift assay to study the binding of ATP and ADP to Cdc123 from yeast and human. The results show that ATP is tightly bound to Cdc123 whereas the affinity of ADP is much smaller. Using yeast cell viability experiments, western blot analysis and two-hybrid assays, we show that ATP is important for the function of Hs-Cdc123 in eIF2 assembly. These data and recent findings (Chen et al., 2023; Vanselow et al., 2022) allow us to propose a refined model to explain the mechanism of action of Cdc123 in eIF2 assembly.

Materials and Methods

Production and purification of Cdc123

The coding sequence of Hs-Cdc123 was amplified by PCR using a Hs-Cdc123 cDNA plasmid (Vanselow et al., 2022) and cloned into NdeI and NotI restriction sites of pET15blpa. The resulting plasmid, pET15b-Hs-Cdc123 allows expression of an N-terminally tagged version of Hs-Cdc123. The plasmid was transformed into *E. coli* BL21 Rosetta pLacI-Rare (Merck, Novagen). 1 L cultures were in 2xTY containing 50 µg/mL of ampicillin and 34 µg/mL of chloramphenicol. Expression was induced by adding 1 mM of IPTG in an overnight 37°C culture. After induction, the cultures were continued for 5 hours at 18°C. For Hs-Cdc123, cells corresponding to 1 L of culture were disrupted by sonication in 40 mL of buffer A (10 mM HEPES pH 7.5, 500 mM NaCl, 3 mM 2-mercaptoethanol, 0.1 mM PMSF, 0.1 mM benzamidine). The crude extract was loaded onto a column (5 mL) containing Talon affinity resin (Clontech) equilibrated in buffer A. After washing the column with buffer A supplemented with 10 mM imidazole, the tagged protein was eluted with buffer A supplemented with 125 mM imidazole. The eluted protein was diluted to reach a 200 mM NaCl concentration and then loaded onto a Q-Sepharose column (10 mm x 4 cm; GE-Healthcare) equilibrated in buffer A1 (10 mM HEPES pH 7.5, 3 mM 2-mercaptoethanol, 0.1 mM PMSF, 0.1 mM benzamidine) supplemented with 200 mM NaCl. A gradient from 200 mM NaCl to 1 M NaCl was used for elution (200 mL at a flow rate of 2.5 mL/min). The recovered protein was finally loaded onto a Superdex 200 10/300 (GE-Healthcare) equilibrated in buffer A1 supplemented with 200 mM NaCl. Hs-Cdc123 was finally concentrated to 10 mg/mL using centricon 30. The same protocol was used to purify Sp-Cdc123 (Panvert et al., 2015) and Sc-Cdc123 (Supplementary Figure 1A).

Production and purification of the human Hs-Cdc123:Hs-γD3 complex

The gene coding for human eIF2γ was first PCR amplified from cDNA and cloned into the NdeI-XhoI restriction sites of the pColaDuet-1-ORF2. The resulting plasmid was then modified using standard QuikChange™ site-directed mutagenesis (Stratagene) to produce a gene fragment coding for the γD3 domain (residues 362-471) of human eIF2γ. The corresponding plasmid was named pColaDuet-

1-ORF2-H-eIF2γD3. pColaDuet-1-ORF2-H-eIF2γD3 and pET15b-Hs-Cdc123 were co-transformed into *E. coli* BL21 Rosetta pLacI-Rare (Merck, Novagen) and selected onto LB plates containing 50 µg/mL of ampicillin, 34 µg/mL of chloramphenicol and 25 µg/mL kanamycin. 1 L cultures were in 2xTY containing the desired antibiotics. Expression was induced by adding 1 mM of IPTG when OD_{650} nm reached 0.8. After induction, the cultures were continued overnight at 18°C. Cells corresponding to 1 L of culture were disrupted by sonication in 40 mL of buffer A. The crude extract was loaded onto a column (5 mL) containing Talon affinity resin (Clontech) equilibrated in buffer A. After washing the column with buffer A supplemented with 10 mM imidazole, the tagged protein was eluted with buffer A supplemented with 125 mM imidazole. The eluted protein was diluted in buffer A1 to reach 200 mM NaCl concentration and then loaded onto a Q-Sepharose column (10 mm x 4 cm; GE-Healthcare) equilibrated in the same buffer. A gradient from 200 mM NaCl to 1 M NaCl was used for elution (200 mL at a flow rate of 2.5 mL/min). This step allowed us to separate the Hs-Cdc123:γD3 complex from the large excess of Hs-Cdc123 isolated after Talon affinity purification. The recovered Hs-Cdc123:γD3 complex was finally loaded onto a Superdex 200 10/300 column (GE-Healthcare) equilibrated in buffer A containing 200 mM NaCl to polish purification of the complex. Finally, Hs-Cdc123:γD3 was concentrated to 10 mg/mL using centricon 30 before crystallization (Supplementary Figure 1A).

To facilitate structure resolution, we also produced and purified Hs-Cdc123:γD3 containing selenomethionine. The selenomethionylated proteins were epressed in autoinducible medium as described (Studier, 2005). After cultivation, the selenomethionylated protein complex was purified as described for native Hs-Cdc123:γD3.

Crystallization and structure determination

Crystallization trials were performed at 4°C with or without 1 mM ATP and 5 mM $MgCl_2$. Sitting drops were made with a Mosquito robot (TTP Labtech) and standard commercial kits (Hampton Research and Qiagen) by mixing 1:1 Hs-Cdc123:γD3 w/wo 1 mM ATP and 5 mM $MgCl_2$ and the precipitating solution. Crystals for native or selenomethionylated Hs-Cdc123:γD3 were rapidly obtained in many different conditions containing PEG3350 (PEG/ION and Index Hampton Research). Before

data collection, the crystals were rapidly soaked into a solution containing the precipitating agent supplemented with 25 to 30% of glycerol. Two X-ray crystallographic datasets collected at the Soleil Synchrotron (Saint Aubin France) on the Proxima-2 beamline were used in this study (Table 1). One dataset was collected from a crystal obtained with selenomethionylated Hs-Cdc123:γD3 with no added ATP-Mg^{2+} and a second dataset was collected from a crystal of Hs-Cdc123:γD3 obtained in the presence of 1 mM ATP and 5 mM Mg^{2+}. Data were processed with XDS (Kabsch, 2010), scaled with AIMLESS (Evans and Murshudov, 2013), analyzed with CCP4 programs (Winn et al., 2011) and finally processed for anisotropy in STARANISO (Tickle et al., 2016). All these steps were performed in AUTOPROC (Vonrhein et al., 2018). Crystals belong to the $P2_1$ space group. However, there is a two-fold NCS axis yielding a strong pseudo $P2_12_12$ symmetry. The structure of Hs-Cdc123:γD3 complex was solved by molecular replacement with PHASER (McCoy et al., 2007) using two separate ensembles, one corresponding to Sp-Cdc123 and the second one to the Sc-γD3 domain (Panvert et al., 2015, PDB ID Code 4ZGQ). For each ensemble, a solution with a high Z-score value was found (Z=8.9 and Z=16.7). The molecular replacement 2mFo-DFc electron density map was of good quality and allowed us to build a first model of Hs-Cdc123:γD3. To facilitate the refinement process, we also calculated an experimental map using the automated SAD phasing procedure with a partial model in Phaser-EP (McCoy et al., 2007; Winn et al., 2011). Coordinates and associated B factors were then refined through several cycles of manual adjustments with Coot (Emsley et al., 2010) and positional refinement with PHENIX (Adams et al., 2010). A small fraction of twinning was evidenced and refined in PHENIX. Moreover, residual electron density showed that some ATP-Mg^{2+} was present in the selenomethionylated Hs-Cdc123:γD3 crystals. Therefore ATP-Mg^{2+} was positioned in the model and the occupancy of the molecule was refined. In the final models, regions 50-68, 294-299 and 311-318 of Hs-Cdc123 and regions 384-390 and 466-470 of Hs-γD3 belonging to long mobile loops could not be traced in the electron density. Statistics for data collection and refinement are given in Supplementary Table 1.

Binding of ATP to Cdc123 using fluorescence-based thermal shift assays

Experiments were done in 96-well plates using a Bio-Rad CFX-96 Real-Time PCR system. Reaction mixtures (25 µL) were assembled in buffer A (10 mM HEPES-NaOH pH 7.5, 500 mM NaCl, 2 mM $MgCl_2$, 10 mM 2-mercaptoethanol) and contained Cdc123 (0.15 mg/mL), 5x SYPRO™ orange (Invitrogen) and various concentrations of ATP-Mg^{2+} (0.1 µM to 6.4 mM). Temperature was increased by 0.5°C every 60 seconds. Fluorescence curves as a function of temperature in the 10°C-70°C range were processed as described (Pantoliano et al., 2001; Redhead et al., 2015), by non-linear least square fitting of the following equation 1 to the experimental datapoints (Supplementary Figure 1B), using Origin (OriginLab) or Prism (GraphPad):

$$F(T) = F_u + m_u(T - T_m) + \frac{F_f - F_u + (T - T_m)(m_f - m_u)}{1 + \exp\left(-\frac{\Delta H_u}{R}\left(\frac{1}{T} - \frac{1}{T_m}\right) + \frac{\Delta Cp_u}{R}\left(\ln\left(\frac{T}{T_m}\right) + \frac{T_m}{T} - 1\right)\right)}$$

F(T) is the measured fluorescence in arbitrary units at the temperature *T*; F_u and F_f are the fluorescence at the melting temperature T_m with the protein in the unfolded and folded states, respectively; m_u and m_f are coefficients reflecting temperature dependence of the fluorescence of the dye bound to the unfolded and folded states, respectively; ΔH_u and ΔCp_u are the enthalpy and heat capacity, respectively, of protein unfolding at a reference temperature chosen as T_m in the absence of ligand and R is the gas constant. Usually, all parameters were allowed to vary in the fitting procedure. In the case of Sc-Cdc123, that had a lower melting temperature than the two other orthologues, m_f was poorly defined for curves recorded at low ATP concentrations and was therefore kept at a constant value of 0 throughout, consistent with the shape of the fluorescence curves at high ATP concentration. In the case of the *Schizosaccharomyces pombe* protein (Sp-Cdc123,) in addition to the main fluorescence transition that occurred around 52°C, a minor fluorescence increase was observed around 80°C. This suggested the existence of an additional minor denaturation step. Only the main transition was considered for T_m calculations (Supplementary Figure 1C).

The obtained T_m values were then used to estimate the dissociation constant of the studied enzyme-ligand couple as described (Cimmperman et al., 2008; Matulis et al., 2005; Pantoliano et al.,

2001; Redhead et al., 2015; Zubrienė et al., 2009). Briefly, the equilibrium constant for protein unfolding at a temperature T can be expressed as:

$$K_u = \exp(-\frac{\Delta H_u}{R}\left(\frac{1}{T} - \frac{1}{T_r}\right) + \frac{\Delta Cp_u}{R}(\frac{T_r}{T} - 1 + \ln\left(\frac{T}{T_r}\right)))$$

where ΔH_u and ΔCp_u are the enthalpy and heat capacity, respectively, of protein unfolding at a reference temperature T_r chosen as T_m in the absence of ligands. Moreover, the binding constant of the ligand at temperature T can be expressed as:

$$K_b = \frac{1}{K_d}\exp(\frac{\Delta H_b}{R}(\frac{1}{T_o} - \frac{1}{T}) - \frac{\Delta Cp_b}{R}(-\frac{T_o}{T} + 1 + \ln\left(\frac{T_o}{T}\right)))$$

where ΔH_b and ΔCp_b are the enthalpy and heat capacity, respectively, of binding of the ligand to the protein unfolding at a reference temperature T_0 chosen as 298K here, and K_d is the dissociation constant of the protein:ligand complex at T_0. The total concentration of ligand in the assay $[L_t]$ necessary to raise the melting temperature to a temperature T can be expressed as (equation 2):

$$[L_t] = (K_u - 1)(\frac{[\mathrm{P}_t]}{2K_u} + \frac{1}{K_b})$$

where $[P_t]$ is the total protein concentration in the assay.

For estimating K_d values, curves simulating the variation of melting temperature as a function of $[L_t]$ were calculated using equation 2 for various K_d values and visually compared with the experimental curves. In this procedure, ΔH_u and ΔCp_u were set to the mean of the values obtained from the fluorescence curves obtained with the control experiments in the absence of ligands. In some cases, for better fitting the whole data, the *Tr* value was slightly adjusted. Each experiment was repeated at least twice, and the means ± sd of the melting temperatures were plotted as a function of the logarithm of ligand concentration. ΔH_b was set to -3 kcal.mol^{-1}, the value measured for ATP binding to Sp-Cdc123 using Isothermal Titration Calorimetry (Panvert et al., 2015) and ΔCp_b to -0.2 kcal.mol^{-1}.K^{-1}, an average value for protein-ligand interactions (Matulis et al., 2005). Note that when varied in realistic ranges, the values of ΔH_b and ΔCp_b did not have a large influence on the K_d estimates (less than a factor of two).

Yeast methods

Standard protocols were followed for growth of budding yeast cells, transformation, sporulation and tetrade dissection (Ausubel et al., 2005). Yeast strains are derivatives of W303 and listed in Supplementary Table 2. Preparation of yeast cell extracts, immunoprecipitation of flag-tagged proteins and Western analysis were done as described (Panvert et al., 2015; Vanselow et al., 2022). For detection of the flag and myc epitopes mouse monoclonal antibodies were used (anti-flag M2; anti-myc 9E10). Sc-eIF2β and Sc-eIF2γ were detected by antisera raised in rabbits (Perzlmaier et al., 2013). In the yeast-two-hybrid vectors pEG202 and pJG4-5 (Ausubel et al., 2005) the human eIF2α encoding cDNA was fused to a lexA-DNA binding domain sequence (pWS4018) and the human eIF2γ encoding cDNA was fused to the B42 transcriptional activator sequence (pWS4023). The human eIF2α and eIF2γ cDNAs were obtained from the DNASU plasmid repository. In addition to the regular reporter strain W276, derivatives expressing Hs-Cdc123 wild type (W15327) or the mutant versions Hs-Cdc123-D233A (W15328) and Hs-Cdc123-D246A (W15329) were used. The mutant alleles of the Hs-Cdc123 gene were created by site-directed mutagenesis (QuickChange; Stratagene). To visualize β-galactosidase production following activation of the *lex*A-operator controlled *lac*Z gene in W276 and its derivatives, yeast colonies were overlaid with an X-Gal top agar (0.2 mg/ml X-Gal; 0.5 M sodium phosphate buffer pH 7.0; 0.1% SDS; 6% DMFA; 0.5% Bacto agar).

RESULTS

Binding of ATP or ADP to Cdc123 using thermal shift assay

In order to study the binding of ATP-Mg^{2+} to Cdc123, we used a thermal shift assay. This method is based on the general idea that ligand binding increases protein stability (Pantoliano et al., 2001). Protein denaturation caused by increasing temperature was monitored using the ThermoFluor™ method with an environmentally sensitive fluorescent dye, allowing us to determine the protein melting temperature T_m (Pinz et al., 2022). This experiment was repeated in the presence of various concentrations of ATP-Mg^{2+} (Supplementary Figure 1B). From the analysis of the variations of the melting temperatures as a function of the concentrations of the nucleotide, dissociation constants can be derived ((Cimmperman et al., 2008; Matulis et al., 2005; Pantoliano et al., 2001; Redhead et al., 2015; Zubrienė et al., 2009); see Materials and methods).

	Estimated *Kd* (µM) ATP	Estimated *Kd* (µM) ADP
Hs-Cdc123	1.6 (17°C)	120 (13°C)
Sc-Cdc123	1.2 (18°C)	18 (11°C)
Sp-Cdc123	140 (6°C)	900 (4°C)

Table 1 : *Kd* values of the ATP and ADP nucleotides for the indicated Cdc123 enzymes.
Values in parentheses show the amplitudes of *Tm* variation in the range of nucleotide concentrations used in the thermal shift assay.

A K_d value of 140 µM could be estimated for the Sp-Cdc123:ATP-Mg^{2+} complex (Figure 1 and Table 1), in reasonable agreement with the value determined using Isothermal Titration Calorimetry (67 µM; (Panvert et al., 2015)). With Sc-Cdc123 and Hs-Cdc123, small concentrations of ATP-Mg^{2+} -in the micromolar range- had larger effects of the stabilities of the proteins as compared to Sp-Cdc123. Consistent with these observations, the estimated dissociation constants were 1.6 µM and 1.2 µM for Hs-Cdc123 and Sc-Cdc123 (Table 1). As compared to ATP-Mg^{2+}, larger concentrations of ADP-Mg^{2+} were required to observe changes in the melting temperature of the three Cdc123 proteins. Accordingly,

the estimated dissociation constants were systematically increased to values of 120 µM (Hs-Cdc123), 18 µM (Sc-Cdc123) and 900 µM (Sp-Cdc123) (Table1).

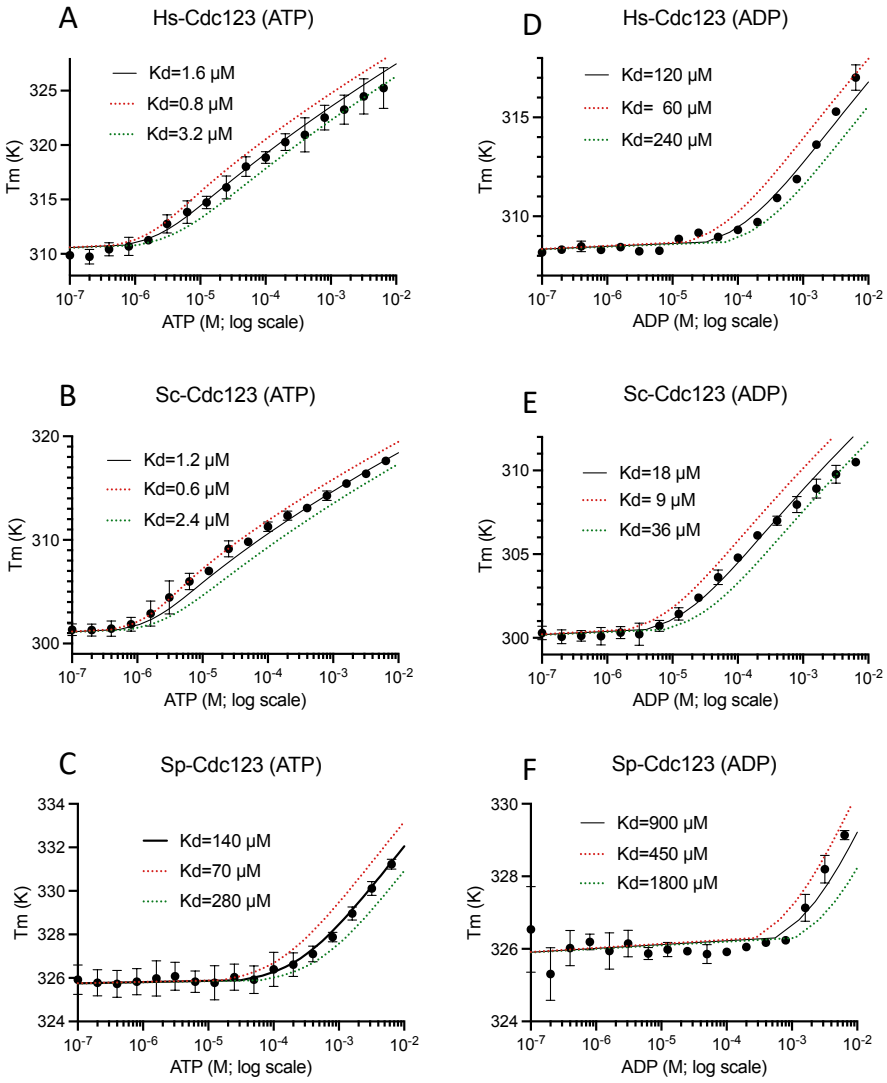

Figure 1: Estimation of *Kd* values.
Each panel plots the measured *Tm* value (mean ± sd from at least two experiments) as a function of the nucleotide concentration in log scale. The best fit to a curve calculated as described in Materials and Methods (Cimmperman et al., 2008; Matulis et al., 2005; Pantoliano et al., 2001; Redhead et al., 2015; Zubrienė et al., 2009) is drawn with a solid line. The corresponding *Kd* value is shown on the panel. Curves obtained with a *Kd* value two-fold higher (green) or two-fold lower (red) are also drawn for comparison. Panels A, B, C: ATP binding to Hs-Cdc123, Sc-Cdc123 and Sp-Cdc123, respectively. Panels D, E, F: same for ADP binding. The estimated dissociation constants are shown in Table 1.

Crystallographic structure of Hs-Cdc123:eIF2γD3 complex

The Hs-Cdc123:eIF2γD3 complex was first purified by affinity chromatography using an N-terminally tagged version of Hs-Cdc123 to trap Hs-eIF2γD3 (See Materials and Methods). Additional steps using anion exchange chromatography and molecular sieving allowed us to polish the preparation (Supplementary Figure 1A). Crystals of Hs-Cdc123:γD3 were obtained at 4°C in solutions containing 20% PEG3350 and various additives, in the presence or in the absence of ATP-Mg^{2+} (Table 1). The structure was solved by molecular replacement and experimental phasing using a selenomethionine version of the complex. Data were processed with STARANISO to deal with diffraction anisotropy. The structure of Hs-Cdc123:γD3:ATP-Mg^{2+} was refined to 2.08 Å resolution and the structure of the selenomethionylated complex was refined to 1.97 Å resolution (Supplementary Table 1). Two molecules related by a pseudo two-fold axis are present in the asymmetric unit. Because the quality of the electron density is slightly better for monomers C and D of Hs-Cdc123 and Hs-γD3, particularly for the long loops of Hs-Cdc123, these two molecules are hereafter used as references. On the other hand, comparison of the structure of the selenomethionylated complex to that of Hs-Cdc123:γD3:ATP-Mg^{2+} complex did not reveal major conformational changes (rms value of 0.267 Å for 357 C-α atoms compared). Therefore, the Hs-Cdc123:γD3:ATP-Mg^{2+} will be majorily described.

Binding of Hs-γD3 to Hs-Cdc123

Hs-Cdc123 is composed of two domains with ATP-Mg^{2+} bound at the interface, as observed in Sp-Cdc123 (Panvert et al., 2015) and in enzymes belonging to the ATP-grasp family (Fawaz et al., 2011) (Figure 2A and Supplementary Figure 2A). D3 of Hs-eIF2γ forms a β barrel highly homologous to its eukaryotic orthologs (Supplementary Figure 3A). It is mainly bound to domain I of Hs-Cdc123 (Figure 2A and 2B).

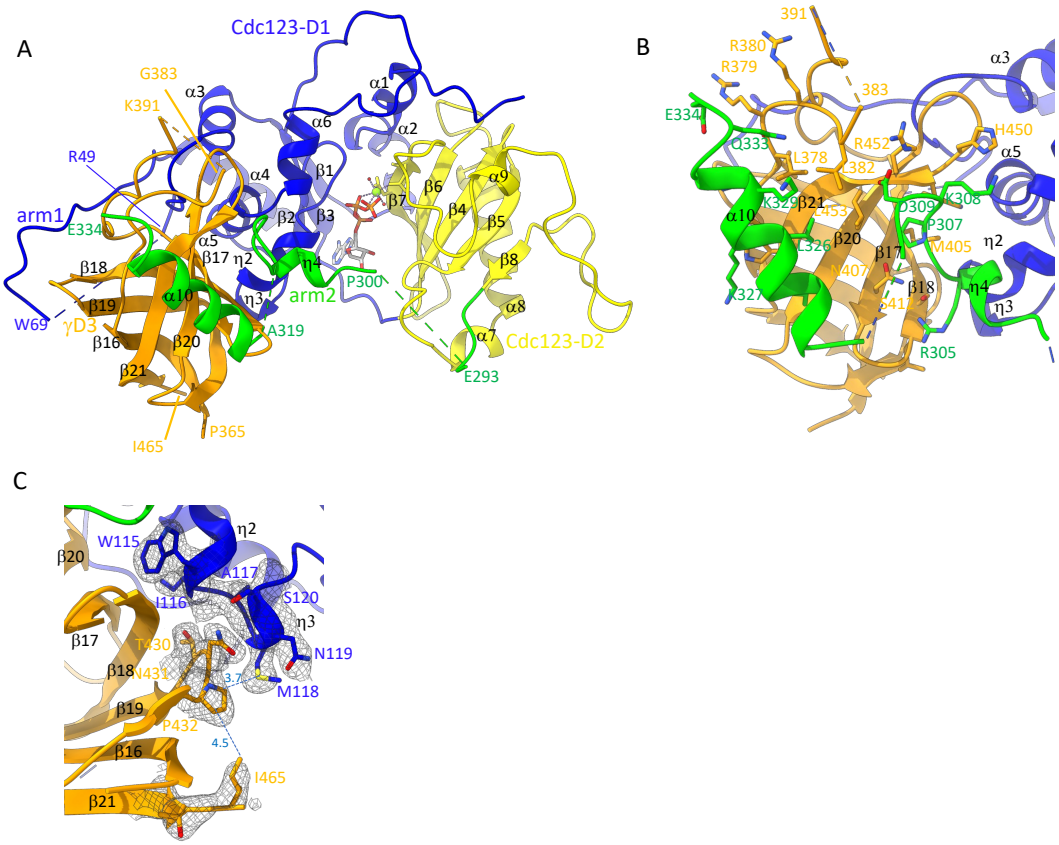

Figure 2: Crystallographic structure of Hs-Cdc123:Hs-γD3:ATP-Mg^{2+}

(A) Overall structure of Hs-Cdc123:γD3:ATP-Mg^{2+}. Hs-Cdc123 is shown in blue (residues 1-174), yellow (residues 175-289) and green (C-terminal peptide, residues 290-336). Regions 50-68, 294-299 and 311-318 of Hs-cdc123 are highly mobile and could not be traced in the electron density. ATP is shown with sticks, Mg^{2+} ion is shown as a green sphere. Hexacoordination of the Mg^{2+} ion is shown with dashed lines (see also Supplementary Figure 4). Hs-γD3 is shown in orange. Secondary structures are labeled as defined for the Sp-Cdc123 structure (Panvert et al., 2015). The figures were made with ChimeraX (Pettersen et al., 2021).

(B) Close-up view of the binding of the C-terminal region of Hs-Cdc123 to Hs-eIF2γD3. Interacting residues belonging to these regions (as listed in Supplementary Table 3) are in sticks and labeled.

(C) Close-up view showing the hydrophobic interaction of P432 with M118 and the proximity of I465 from P432. Interactions involving T430, N431 and P432 with residues from the h2-h3 helices of Cdc123 are listed in Supplementary Table 3.

The η2–η3, α6 and the 39-43 loop of Hs-Cdc123 carry residues involved in the interaction with Hs-γD3 (Supplementary Table 3). Overall, the structure of Hs-Cdc123:γD3:ATP-Mg^{2+} is similar to the previously determined structure of Sp-Cdc123:Sc-γD3 complex (Panvert et al., 2015) (rmsd between the two structures is 1.2 Å for 299 Cα atoms compared). This shows that the main regions of contact between γD3 and domain I of Cdc123 are similar in the two structures (Supplementary Figure 2A) and conserved from yeast to human. When the Cdc123 molecules of the human and yeast complexes are superimposed, a small difference in the positioning of the γD3 domain with respect to Cdc123-D1 is

observed (3.06 Å translation and 9.6° rotation, Supplementary Figure 2A). This difference in the orientation of γD3 is possibly related to a small movement of Cdc123 α3 and the following loop as well as to the participation of C-terminal region of Hs-Cdc123 in the binding to γD3 (Figure 2B). Indeed, in Hs-Cdc123 domain I, the long linker containing forty-four residues located between α3 and α4 (residues 40-83, Supplementary Figure 2) is partially ordered. Residues 40-50 and 69-83 were positioned in the electron density (Supplementary Figure 4). This region surrounds γD3 and contacts it on the side of the β18-β19 hairpin. This region is hereafter named arm 1 (Figure 2). On the other hand, the C-terminal region of Hs-Cdc123 could be partially built (Figure 2 and Supplementary Figure 4 A-C). This long C-terminal tail, from residue 290 to residue 336, starts from Hs-Cdc123 domain 2 and extends to Hs-γD3 with which it interacts via its C-terminal α-helix. This region is hereafter named arm 2. These two regions contribute many interactions described in Supplementary Table 3. Arm1 and arm2 of Hs-Cdc123 act as tweezers that wrap the Hs-γD3 domain and increase the surface of interaction between Cdc123 and γD3 to 4530 $Å^2$, as compared to 1307 $Å^2$ for the Sp-Cdc123:Sc-γD3 complex or 1742 $Å^2$ for the present complex where regions 69-80 and 291-336 have been deleted from the model (Supplementary Figure 2B). These two regions have B-values above the mean B-values for the model (Supplementary Figure 2C) indicative of their flexibility. Packing analysis shows that region from residue 290 to 319 of Hs-Cdc123 is not involved in packing interactions in the crystals. However, the C-terminal α10 helix of one Hs-Cdc123 also contacts a neighbor molecule. Therefore, its positioning could have been stabilized by crystal packing interactions. In the Sp-Cdc123:Sc-γD3 structure, arm 2 was mostly disordered and only the C-terminal helix could be built. However, the positioning of this C-terminal helix with respect to the main part of Cdc123 could not be established. Overall, the present data suggests that these two arms are mobile regions of Cdc123 that are involved in the binding of the γD3 domain.

ATP-Mg^{2+} binding site of Hs-Cdc123

ATP-Mg^{2+} is bound to Hs-Cdc123 at the interface between D1 and D2. Residues involved in ATP-Mg^{2+} binding were analyzed with Ligplot (Wallace et al., 1996) and shown in Figure 3A. For

comparison, the Sp-Cdc123 structure bound to ATP-Mg^{2+} is shown in Figure 3B. Most residues involved in ATP binding are conserved in the two proteins (Supplementary Figure 3).

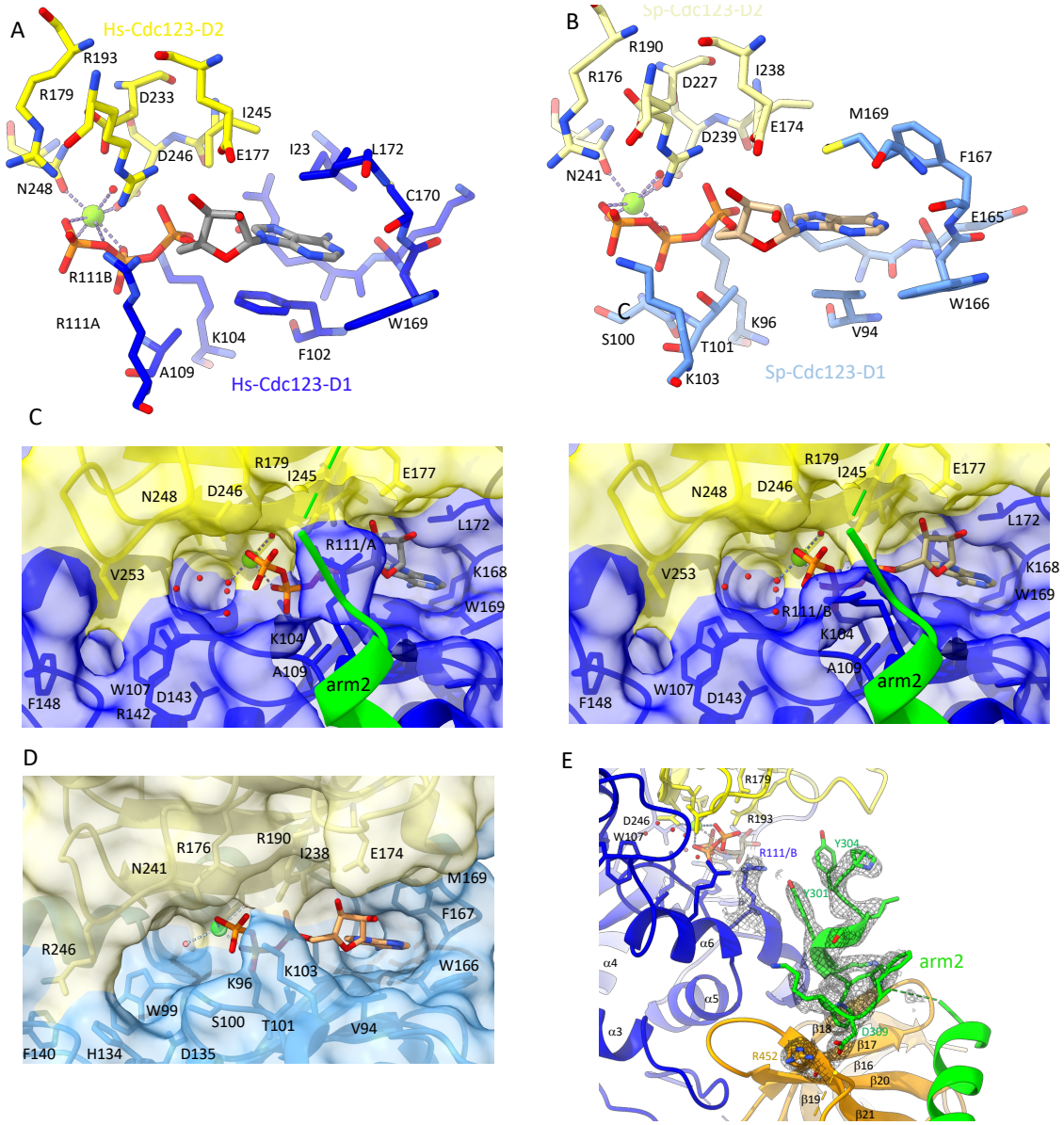

Figure 3: Binding of ATP-Mg^{2+}

(A) The Hs-Cdc123 residues involved in ATP binding are shown in sticks. D233 (D227 in Sp-Cdc123) is also represented as it tightly interacts with R179, N248, and a water molecule (see also Supplementary Figure 4D). Residues belonging to domain 1 are colored in blue and those belonging to domain II are colored in yellow. Water molecules are shown with red spheres and the magnesium ion is shown as a green sphere.

(B) Same as view A but for Sp-Cdc123 (Panvert et al., 2015).

(C) Molecular surface representation of Hs-Cdc123:Hs-γD3 :ATP-Mg^{2+}. The color code is the same as in view A. The view shows the cavity facing the ATP binding pocket with the side chain of R111 in two alternative conformations (A, right and B, left).

(D) Same as C but for Sp-Cdc123:Sc-γD3:ATP-Mg^{2+}.

(E) Close-up view showing the contacts of Hs-Cdc123 arm 2 with the ATP binding site and with γD3.

To address the relevance of ATP binding to the human Cdc123 ortholog, we generated two variants altered in the ATP-binding site and studied their properties. To this end, we replaced two conserved aspartate residues (D233 and D246 in Hs-Cdc123 corresponding to D227 and D239 in Sp-Cdc123, Panvert et al., 2015); Figure 3A and B, Supplementary Figure 3) by alanine residues through site-directed mutagenesis of the Hs-Cdc123 gene. In a first step, we tested for biological function by complementation analysis in budding yeast. For this, we expressed wild type Hs-Cdc123 and the mutant versions D233A and D246A in a diploid yeast strain heterozygote for a *CDC123* gene deletion. Western analysis confirmed that the mutant Hs-Cdc123 versions were expressed at levels comparable to the wild type protein (Figure 4A). By tetrade dissection following meiosis and sporulation, we recovered haploid progeny carrying a Hs-Cdc123 expression construct but lacking the yeast *CDC123* gene. In case of wild type Cdc123, these cells had normal growth properties as indicated by the formation of regular sized colonies (Figure 4A). Apparently, Hs-Cdc123 can take over the function of its yeast ortholog consistent with a previous systematic gene replacement study (Kachroo et al., 2015). In contrast, yeast *cdc123*-Δ cells expressing the Hs-Cdc123-D233A or -D246A mutant version formed only tiny or small colonies, respectively (Figure 4A). These data suggest that the biological function of Hs-Cdc123 depends on the integrity of its ATP binding site.

To define further the defect caused by a compromised ATP binding site, we studied the interaction of the Hs-Cdc123 mutant proteins with eIF2 subunits. For this, flag-tagged Hs-Cdc123 constructs were expressed in yeast and a strain expressing flag-tagged yeast Cdc123 served as a positive control. Flag-tagged proteins were immunoprecipitated from cell extracts and analyzed for co-precipitation of eIF2 subunits by Western analysis. Precipitates of Hs-Cdc123 contained eIF2 subunits in amounts similar to precipitates of Sc-Cdc123 (Figure 4B). In contrast, the mutant versions of Hs-Cdc123 co-precipitated hardly any (D233A) or only very little (D246A) of the β and γ subunits of eIF2 consistent with the view that integrity of the ATP binding site of Cdc123 is essential for the interaction of Cdc123 with eIF2γ and the eIF2γ-eIF2β dimer (Panvert et al., 2015; Vanselow et al., 2022). To facilitate detection of Sc-eIF2α, the yeast strains used in this analysis carried a myc-epitope fusion of the *SUI2* gene, which encodes eIF2α in budding yeast. The myc-tagged Sc-eIF2α subunit was present

in similar amounts in the precipitates of Sc-Cdc123 and both the wild type and mutant versions of Hs-Cdc123. This confirms a previously observed direct contact of Sc-Cdc123 with Sc-eIF2α (Vanselow et al., 2022) and suggests that the Cdc123-eIF2α contact does not require intactness of the ATP binding site of Cdc123.

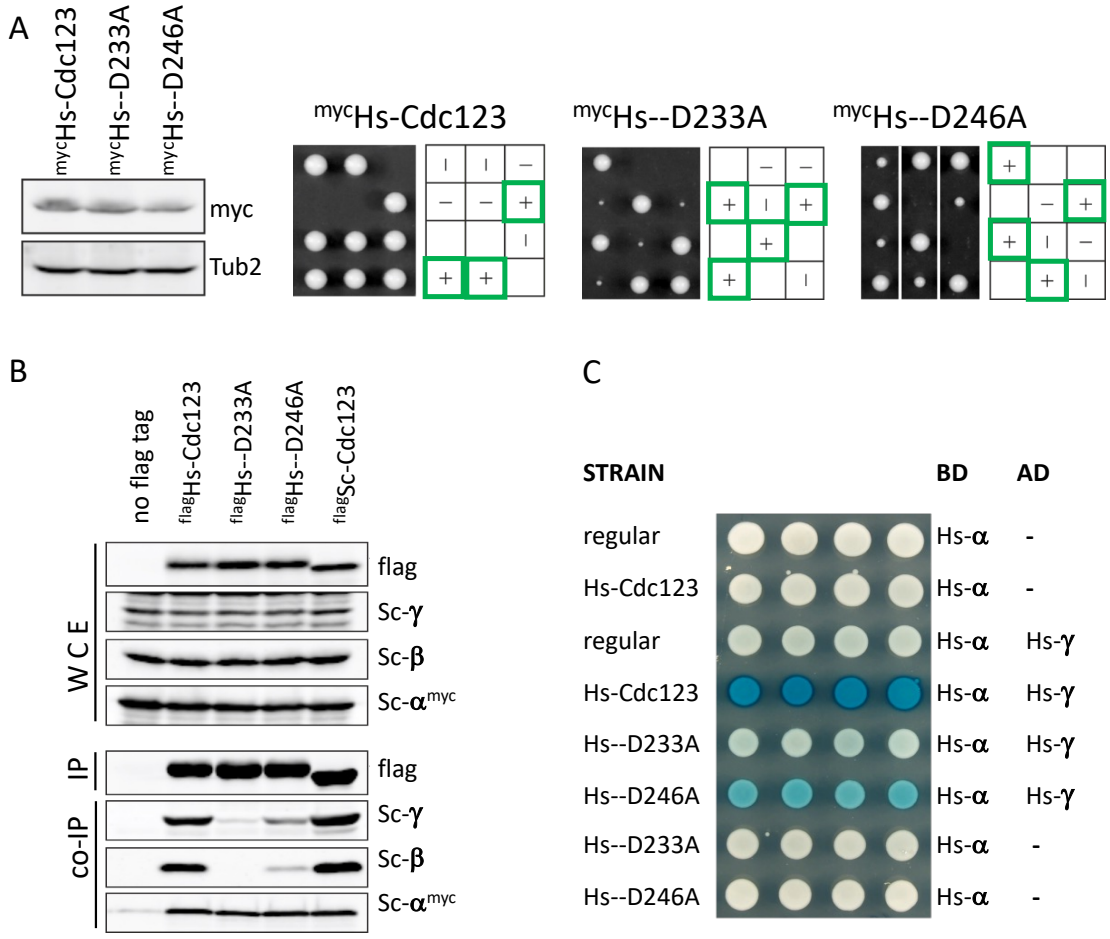

Figure 4: ATP binding site variants of Hs-Cdc123.

(A) Complementation analysis in yeast. Expression of myc-tagged wild type or mutant versions of Hs-Cdc123 in CDC123/cdc123-Δ diploid strains (Hs-Cdc123: W15001; Hs-Cdc123-D233A: W15002; Hs-Cdc123-D246A: W15003) was compared by Western analysis. Tub2 served as a protein loading control. The four haploid spores generated by a single diploid cell were recovered by tetrade dissection and placed in a vertical line on solid growth medium to monitor colony formation. Green squares indicate the positions of haploid progeny carrying both the cdc123-□ allele (horizontal line) and the Hs-Cdc123 expression construct (vertical line).

(B) Hs-Cdc123 protein interaction with Sc-eIF2 subunits. Expression of flag-tagged wild type or mutant versions of Hs-Cdc123 in a SUI2-myc strain (Hs-Cdc123: W14968; Hs-Cdc123-D233A: W14969; Hs-Cdc123-D246A: W14970) was inspected by Western analysis. Negative and positive controls were the SUI2-myc strain lacking a flag expression construct (no flag tag: W9877) or expressing flag-tagged Sc-Cdc123 (W14974), respectively. Whole cell extracts (WCE) of these strains were also probed for Sc-eIF2γ, Sc-eIF2β and Sc-eIF2α-myc. From the whole cell extracts, flag-tagged proteins were immunoprecipitated by an antibody against the flag

epitope (IP). These precipitates were probed by Western analysis for the presence of flag-tagged proteins, Sc-eIF2γ, Sc-eIF2β and Sc-eIF2α-myc (co-IP).

(C) Yeast-two-hybrid analysis of Hs-eIF2γ association with Hs-eIF2α. Y2H-reporter strains that lack any Hs-Cdc123 construct (regular: W276) or express flag-tagged wild type (Hs-Cdc123: W15327) or mutant versions (Hs--D233A: W15328; Hs--D246A: W15328) of Hs-Cdc123 were used to express the lexA DNA binding domain (BD) fused human eIF2α subunit (Hs-α) either alone to test for autoactivation or in combination with a B42 transcriptional activation domain (AD) fused human eIF2γ subunit (Hs-γ) to test for association of Hs-eIF2α with Hs-eIF2γ. Yeast colonies were overlaid with a X-gal containing top agar to visualize β-galactosidase activity resulting from transcriptional activation of the lexAop-lacZ reporter gene.

As a third test, we analyzed the ability of Hs-Cdc123 to promote eIF2 assembly. For this, we used a Y2H-assay to monitor the association of Hs-eIF2α fused to a DNA-binding domain with Hs-eIF2γ fused to a transcriptional activation domain. Co-expression of the human α and γ subunits activated the *lac*Z reporter gene only weakly (Figure 4C). Interestingly, the additional expression of wild type Hs-Cdc123 in the Y2H strain increased the reporter signal substantially. This suggests that Hs-Cdc123 can promote assembly of human eIF2 subunits in yeast. In contrast, the ATP binding site mutants of Hs-Cdc123 had either marginal (D233A) or significantly reduced (D246A) activity in this assembly assay. Together the data point to a critical role of the ATP binding site for the biological function of Hs-Cdc123 and its biochemical activity in eIF2 subunit binding and assembly.

Interestingly, R111 in Hs-Cdc123 replaces K103 of Sp-Cdc123 (Figure 3A and B). R111 shows two alternative side chain conformations that make several interactions with the γ and β phosphate of ATP-Mg^{2+} (Figure 3C and D). These additional contacts could participate in the high binding affinity of Hs-Cdc123 for ATP-Mg^{2+}. An R residue is also found at this position in Sc-Cdc123 which also displays high affinity for ATP (Table 1, Supplementary Figure 3B). As already observed in Sp-Cdc123 (Panvert et al., 2015), a cavity borders the gamma phosphate group of ATP (Figure 3C and D). This cavity, filled with water molecules, may be the binding site of another substrate. The shape of the cavity in Hs-Cdc123 is different from that of Sp-Cdc123 due to some variations in the side chains of residues that border it. Notably, the 300-306 region in the C-terminal of Hs-Cdc123 is located close to R111 and the ATP binding site (Figure 3E). In particular, Y304 contacts the side chain of R111 in its B conformation. Moreover, as mentioned above, the "300" region of Hs-Cdc123 also contacts γD3 and the α10 helix is

packed onto the γD3 barrel. Therefore, the present structure shows a link between the ATP binding site and the binding of the γD3 domain (Figure 3E).

DISCUSSION

Previous results showed that the C-terminal tail of yeast eIF2γ was required for the interaction with yeast Cdc123. Removal of the last 13 amino acids of Sc-eIF2γ rendered eIF2γ unable to co-precipitate Cdc123 or α and β subunits (Perzlmaier et al., 2013). On the other hand, the C-terminal region of yeast Cdc123 is required for its function in vivo (Panvert et al., 2015). Moreover, similarly to the situation in yeast, it was shown using a yeast strain expressing Hs-eIF2 subunits, that the C-terminus of Hs-eIF2γ was also required for interaction with Hs-Cdc123 or Hs-eIF2α or Hs-eIF2β (Vanselow et al., 2022). The present structure shows for the first time the tracing for the C-terminal region of Cdc123 that goes from Cdc123 domain 2 to eIF2γD3 binding site. γD3 interacts with residues 305 to 309 and the C-terminal helix of Cdc123. These two regions contact the face β17-18-20-21 (Figure 2B) of the γD3 β-barrel which overlaps the binding site of domain I of eIF2γ. Therefore, the binding of the C-terminal domain of Cdc123 at this position is not compatible with the binding of the active conformation of eIF2γ as it is observed in the heterotrimeric eIF2 (Brito Querido et al., 2020; Llacer et al., 2015; Schmitt et al., 2012). This observation agrees well with recent conclusions obtained with the yeast proteins that Cdc123 can interrupt the intramolecular association of the G-domain (D1) of eIF2γ with domains 2 and 3 (Vanselow et al., 2022). One could imagine that in a first step, Cdc123 binds an immature form of eIF2γ that prevents its interaction with α and β subunits. This immature conformation may resemble the open form of elongation factor 1A -a protein homologous to eIF2γ (Schmitt et al., 2002)- observed in the presence of GDP (Andersen et al., 2001; Berchtold et al., 1993; Crepin et al., 2014; Kjeldgaard and Nyborg, 1992). Such an open conformation of eIF2γ would be compatible with the binding of Cdc123 as observed here. In a second step, during Cdc123-guided maturation of eIF2γ, the C-terminal part of Cdc123 would be released from its binding site on the γD3 domain allowing eIF2γ to reach its active conformation capable of binding eIF2α and eIF2β (Figure 4). Importantly, the C-terminal part of Cdc123 contacts both the ATP binding pocket and the eIF2γD3 domain. These contacts

may allow Cdc123 to couple eIF2γ binding to ATP consumption. Recent results show that effector-triggered immunity in plants is enhanced by Cdc123 through elevated ATP levels and that impairment of ATP hydrolysis disfavors Cdc123-mediated eIF2 assembly (Chen et al., 2023). This supports the idea that Cdc123 activity might be regulated by ATP concentration.

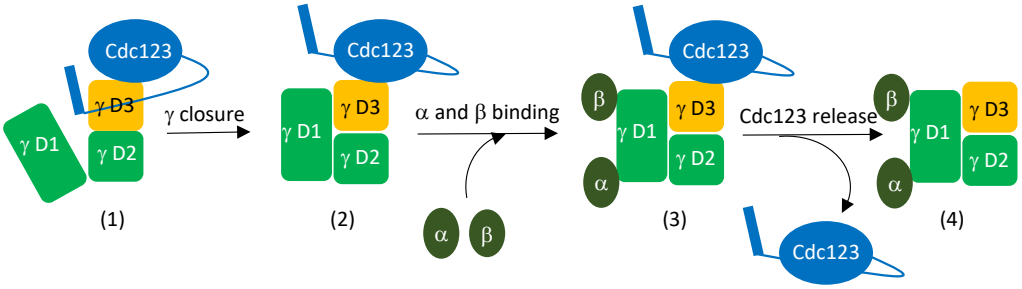

Figure 5: Model of Cdc123-assisted eIF2 assembly.

Cdc123 would bind an open conformation of eIF2γ unable to bind α and β subunits (1). In a second step, during Cdc123-guided maturation of eIF2γ, the C-terminal part of Cdc123 would be released from its binding site on γD3 allowing eIF2γ to reach its active conformation (2). eIF2γ is now capable of binding to α and β (3) triggering Cdc123 release (4). During the process, ATP hydrolysis would occur on Cdc123, which would be released in an ADP-bound form. Because of the lower affinity for ADP (Table 1), Cdc123 would be spontaneously recycled to its ATP-bound form, under the control of intracellular concentration of ATP.

The present work also gives a structural support for interpreting the effects of mutations in eIF2γ gene that are responsible for MEHMO diseases. A P432S mutation in the gene coding for eIF2γ was isolated in patients affected by X-linked hypopituitarism and glucose dysregulation (Gregory et al., 2019). The Hs-Cdc123:γD3 structure shows hydrophobic contacts between P432 of eIF2γD3 and Hs-Cdc123 domain 1 (Figure 2C). Moreover, many interactions between the 430-432 region of eIF2γD3 and η2,η3 Cdc123 helices are observed (Supplementary Table 3). Therefore, it is possible that mutation P432S destabilizes the contacts between eIF2γ and Cdc123 and results in deficiency of Cdc123-assisted eIF2 assembly. The frameshifting mutation, known to impair Cdc123 promotion of eIF2 complex formation, changes the C-terminal sequence of eIF2γ from G_{462}VTIKPTVDD to G_{462}VTSQQ. The last residue visible in the present structure is eIF2γ-I465. Interestingly, I465 side chain is close to P432 (4.5 Å). Thus, the frameshifting mutation may affect contacts between the C-terminal extremity of eIF2γ and Cdc123. To conclude, the present study provides structural basis for the design of new molecules that

could reinforce the interaction of Cdc123 with eIF2γ to compensate for the effect of MEHMO associated mutations.

Data availability

X-ray data and models have been deposited to the Protein Data Bank under the accession numbers 8PHD (Hs-Cdc123:Hs-eIF2γD3:ATP-Mg^{2+}), 8PHV (Hs-Cdc123:Hs-eIF2γD3 selenomethione).

Supplementary Data

Supplementary Data are available.

Funding

This work was supported by grants from the Centre National de la Recherche Scientifique and Ecole Polytechnique to Unité Mixte de Recherche n°7654 and by a grant from the Deutsche Forschungsgemeinschaft (SFB960 project B10) to WS. CCP was a recipient of a PhD fellowship from Institut Polytechnique de Paris.

Acknowledgements

X-ray data were collected at Soleil synchrotron. We thank Pierre Legrand (PX1), William Shepard (PX2), Martin Savko (PX2) and for their help with X-ray data collections on Proxima-1 and Proxima-2 beamlines.

REFERENCES

Adams, P.D., Afonine, P.V., Bunkóczi, G., Chen, V.B., Davis, I.W., Echols, N., Headd, J.J., Hung, L.-W., Kapral, G.J., Grosse-Kunstleve, R.W., McCoy, A.J., Moriarty, N.W., Oeffner, R., Read, R.J., Richardson, D.C., Richardson, J.S., Terwilliger, T.C., H., Z.P., 2010. PHENIX: a comprehensive Python-based system for macromolecular structure solution. Acta Cryst. D66, 213-221.

Andersen, G.R., Valente, L., Pedersen, L., Kinzy, T.G., Nyborg, J., 2001. Crystal structures of nucleotide exchange intermediates in the eEF1A- eEF1Balpha complex. Nat. Struct. Biol. 8, 531-534.

Ausubel, F.M., Brent, R., Kingston, R.E., Moore, D.D., Seidman, J.G., Smith, J.A., Struhl, K., 2005. Current Protocols in Molecular Biology John Wiley &Sons Hoboken, NJ.

Berchtold, H., Reshtnikova, L., Reiser, C.O.A., Schirmer, N.K., Sprinzl, M., Hilgenfeld, R., 1993. Crystal structure of active elongation factor Tu reveals major domain rearrangements. Nature 365, 126-132.

Bieganowski, P., Shilinski, K., Tsichlis, P.N., Brenner, C., 2004. Cdc123 and checkpoint forkhead associated with RING proteins control the cell cycle by controlling eIF2gamma abundance. J Biol Chem 279, 44656-44666.

Borck, G., Shin, B.S., Stiller, B., Mimouni-Bloch, A., Thiele, H., Kim, J.R., Thakur, M., Skinner, C., Aschenbach, L., Smirin-Yosef, P., Har-Zahav, A., Nürnberg, G., Altmüller, J., Frommolt, P., Hofmann, K., Konen, O., Nürnberg, P., Munnich, A., Schwartz, C.E., Gothelf, D., Colleaux, L., Dever, T.E., Kubisch, C., Basel-Vanagaite, L., 2012. eIF2γ mutation that disrupts eIF2 complex integrity links intellectual disability to impaired translation initiation. Mol Cell 48, 641-646.

Brito Querido, J., Sokabe, M., Kraatz, S., Gordiyenko, Y., Skehel, J.M., Fraser, C.S., Ramakrishnan, V., 2020. Structure of a human 48S translational initiation complex. Science 369, 1220-1227.

Chen, T., Xu, G., Mou, R., Greene, G.H., Liu, L., Motley, J., Dong, X., 2023. Global translational induction during NLR-mediated immunity in plants is dynamically regulated by CDC123, an ATP-sensitive protein. Cell Host Microbe 31, 334-342.e335.

Cimmperman, P., Baranauskiene, L., Jachimoviciūte, S., Jachno, J., Torresan, J., Michailoviene, V., Matuliene, J., Sereikaite, J., Bumelis, V., Matulis, D., 2008. A quantitative model of thermal stabilization and destabilization of proteins by ligands. Biophys J 95, 3222-3231.

Crepin, T., Shalak, V.F., Yaremchuk, A.D., Vlasenko, D.O., McCarthy, A., Negrutskii, B.S., Tukalo, M.A., El'skaya, A.V., 2014. Mammalian translation elongation factor eEF1A2: X-ray structure and new features of GDP/GTP exchange mechanism in higher eukaryotes. Nucleic Acids Research 42, 12939-12948.

Dubiez, E., Aleksandrov, A., Lazennec-Schurdevin, C., Mechulam, Y., Schmitt, E., 2015. Identification of a second GTP-bound magnesium ion in archaeal initiation factor 2. Nucleic Acids Res 43, 2946-2957.

Emsley, P., Lohkamp, B., Scott, W.G., Cowtan, K., 2010. Features and development of Coot. Acta Crystallogr. D66, 486-501.

Evans, P.R., Murshudov, G.N., 2013. How good are my data and what is the resolution? Acta Crystallographica Section D 69, 1204-1214.

Fawaz, M.V., Topper, M.E., Firestine, S.M., 2011. The ATP-grasp enzymes. Bioorg Chem 39, 185-191.

Gregory, L.C., Ferreira, C.B., Young-Baird, S.K., Williams, H.J., Harakalova, M., van Haaften, G., Rahman, S.A., Gaston-Massuet, C., Kelberman, D., Gosgene, Qasim, W., Camper, S.A., Dever, T.E., Shah, P., Robinson, I., Dattani, M.T., 2019. Impaired EIF2S3 function associated with a novel phenotype of X-linked hypopituitarism with glucose dysregulation. EBioMedicine 42, 470-480.

Hinnebusch, A.G., 2014. The scanning mechanism of eukaryotic translation initiation. Annu Rev Biochem 83, 779-812.

Ho, Y., Gruhler, A., Heilbut, A., Bader, G.D., Moore, L., Adams, S.L., Millar, A., Taylor, P., Bennett, K., Boutilier, K., Yang, L., Wolting, C., Donaldson, I., Schandorff, S., Shewnarane, J., Vo, M., Taggart, J., Goudreault, M., Muskat, B., Alfarano, C., Dewar, D., Lin, Z., Michalickova, K., Willems, A.R., Sassi, H., Nielsen, P.A., Rasmussen, K.J., Andersen, J.R., Johansen, L.E.,

Hansen, L.H., Jespersen, H., Podtelejnikov, A., Nielsen, E., Crawford, J., Poulsen, V., Sorensen, B.D., Matthiesen, J., Hendrickson, R.C., Gleeson, F., Pawson, T., Moran, M.F., Durocher, D., Mann, M., Hogue, C.W., Figeys, D., Tyers, M., 2002. Systematic identification of protein complexes in Saccharomyces cerevisiae by mass spectrometry. Nature 415, 180-183.

Kabsch, W., 2010. XDS. Acta crystallographica. Section D, Biological crystallography 66, 125-132.

Kachroo, A.H., Laurent, J.M., Yellman, C.M., Meyer, A.G., Wilke, C.O., Marcotte, E.M., 2015. Evolution. Systematic humanization of yeast genes reveals conserved functions and genetic modularity. Science 348, 921-925.

Kazan, R., Bourgeois, G., Lazennec-Schurdevin, C., Coureux, P.D., Mechulam, Y., Schmitt, E., 2023. Structural insights into the evolution of late steps of translation initiation in the three domains of life. Biochimie.

Kjeldgaard, M., Nyborg, J., 1992. Refined structure of elongation factor EF-Tu from Escherichia coli. J. Mol. Biol. 223, 721-742.

Kotzaeridou, U., Young-Baird, S.K., Suckow, V., Thornburg, A.G., Wagner, M., Harting, I., Christ, S., Strom, T., Dever, T.E., Kalscheuer, V.M., 2020. Novel pathogenic EIF2S3 missense variants causing clinically variable MEHMO syndrome with impaired eIF2γ translational function, and literature review. Clin Genet 98, 507-514.

Krishnamoorthy, T., Pavitt, G.D., Zhang, F., Dever, T.E., Hinnebusch, A.G., 2001. Tight binding of the phosphorylated alpha subunit of initiation factor 2 (eIF2alpha) to the regulatory subunits of guanine nucleotide exchange factor eIF2B is required for inhibition of translation initiation. Mol Cell Biol 21, 5018-5030.

Llacer, J.L., Hussain, T., Marler, L., Aitken, C.E., Thakur, A., Lorsch, J.R., Hinnebusch, A.G., Ramakrishnan, V., 2015. Conformational Differences between Open and Closed States of the Eukaryotic Translation Initiation Complex. Mol Cell 59, 399-412.

Matulis, D., Kranz, J.K., Salemme, F.R., Todd, M.J., 2005. Thermodynamic stability of carbonic anhydrase: measurements of binding affinity and stoichiometry using ThermoFluor. Biochemistry 44, 5258-5266.

McCoy, A.J., Grosse-Kunstleve, R.W., Adams, P.D., Winn, M.D., Storoni, L.C., Read, R.J., 2007. Phaser crystallographic software. Journal of Applied Crystallography 40, 658-674.

Moortgat, S., Desir, J., Benoit, V., Boulanger, S., Pendeville, H., Nassogne, M.C., Lederer, D., Maystadt, I., 2016. Two novel EIF2S3 mutations associated with syndromic intellectual disability with severe microcephaly, growth retardation, and epilepsy. Am J Med Genet A 170, 2927-2933.

Pantoliano, M.W., Petrella, E.C., Kwasnoski, J.D., Lobanov, V.S., Myslik, J., Graf, E., Carver, T., Asel, E., Springer, B.A., Lane, P., Salemme, F.R., 2001. High-density miniaturized thermal shift assays as a general strategy for drug discovery. J Biomol Screen 6, 429-440.

Panvert, M., Dubiez, E., Arnold, L., Perez, J., Mechulam, Y., Seufert, W., Schmitt, E., 2015. Cdc123, a Cell Cycle Regulator Needed for eIF2 Assembly, Is an ATP-Grasp Protein with Unique Features. Structure 23, 1596-1608.

Pavitt, G.D., 2018. Regulation of translation initiation factor eIF2B at the hub of the integrated stress response. WIREs RNA 9, e1491.

Perzlmaier, A.F., Richter, F., Seufert, W., 2013. Translation initiation requires cell division cycle 123 (Cdc123) to facilitate biogenesis of the eukaryotic initiation factor 2 (eIF2). J Biol Chem 288, 21537-21546.

Pettersen, E.F., Goddard, T.D., Huang, C.C., Meng, E.C., Couch, G.S., Croll, T.I., Morris, J.H., Ferrin, T.E., 2021. UCSF ChimeraX: Structure visualization for researchers, educators, and developers. Protein Sci 30, 70-82.

Pinz, S., Doskocil, E., Seufert, W., 2022. Thermofluor-Based Analysis of Protein Integrity and Ligand Interactions. Methods Mol Biol 2533, 247-257.

Redhead, M., Satchell, R., Morkūnaitė, V., Swift, D., Petrauskas, V., Golding, E., Onions, S., Matulis, D., Unitt, J., 2015. A combinatorial biophysical approach; FTSA and SPR for identifying small molecule ligands and PAINs. Anal Biochem 479, 63-73.

Schmitt, E., Blanquet, S., Mechulam, Y., 2002. The large subunit of initiation factor aIF2 is a close structural homologue of elongation factors. EMBO J. 21, 1821-1832.

Schmitt, E., Naveau, M., Mechulam, Y., 2010. Eukaryotic and archaeal translation initiation factor 2: a heterotrimeric tRNA carrier. FEBS Lett. 584, 405-412.
Schmitt, E., Coureux, P.-D., Kazan, R., Bourgeois, G., Lazennec-Schurdevin, C., Mechulam, Y., 2020. Recent advances in archaeal translation initiation. Frontiers in Microbiology.
Schmitt, E., Panvert, M., Lazennec-Schurdevin, C., Coureux, P.D., Perez, J., Thompson, A., Mechulam, Y., 2012. Structure of the ternary initiation complex aIF2-GDPNP-methionylated initiator tRNA. Nat. Struct. Mol. Biol. 19, 450-454.
Skopkova, M., Hennig, F., Shin, B.S., Turner, C.E., Stanikova, D., Brennerova, K., Stanik, J., Fischer, U., Henden, L., Muller, U., Steinberger, D., Leshinsky-Silver, E., Bottani, A., Kurdiova, T., Ukropec, J., Nyitrayova, O., Kolnikova, M., Klimes, I., Borck, G., Bahlo, M., Haas, S.A., Kim, J.R., Lotspeich-Cole, L.E., Gasperikova, D., Dever, T.E., Kalscheuer, V.M., 2017. EIF2S3 Mutations Associated with Severe X-Linked Intellectual Disability Syndrome MEHMO. Hum Mutat.
Studier, F.W., 2005. Protein production by auto-induction in high density shaking cultures. Protein Expr Purif 41, 207-234.
Tickle, I.J., Flensburg, C., Keller, P., Paciorek, W., Sharff, A., Vonrhein, C., Bricogne, G., 2016. STARANISO (http://staraniso.globalphasing.org/cgi-bin/staraniso.cgi). Cambridge, United Kingdom: Global Phasing Ltd. .
Vanselow, S., Neumann-Arnold, L., Wojciech-Moock, F., Seufert, W., 2022. Stepwise assembly of the eukaryotic translation initiation factor 2 complex. J Biol Chem 298, 101583.
Vonrhein, C., Tickle, I.J., Flensburg, C., Keller, P., Paciorek, W., Sharff, A., Bricogne, G., 2018. Advances in automated data analysis and processing within autoPROC, combined with improved characterisation, mitigation and visualisation of the anisotropy of diffraction limits using STARANISO. Acta Crystallographica Section A 74, a360.
Wallace, A.C., R.A., L., J.M., T., 1996. LIGPLOT: a program to generate schematic diagrams of protein-ligand interactions. . Protein Eng. 8, 127-134.
Wang, T., Birsoy, K., Hughes, N.W., Krupczak, K.M., Post, Y., Wei, J.J., Lander, E.S., Sabatini, D.M., 2015. Identification and characterization of essential genes in the human genome. Science 350, 1096-1101.
Wek, R.C., 2018. Role of eIF2α Kinases in Translational Control and Adaptation to Cellular Stress. Cold Spring Harb Perspect Biol 10.
Winn, M.D., Ballard, C.C., Cowtan, K.D., Dodson, E.J., Emsley, P., Evans, P.R., Keegan, R.M., Krissinel, E.B., Leslie, A.G., McCoy, A., McNicholas, S.J., Murshudov, G.N., Pannu, N.S., Potterton, E.A., Powell, H.R., Read, R.J., Vagin, A., Wilson, K.S., 2011. Overview of the CCP4 suite and current developments. Acta Crystallogr D Biol Crystallogr 67, 235-242.
Young-Baird, S.K., Shin, B.S., Dever, T.E., 2019. MEHMO syndrome mutation EIF2S3-I259M impairs initiator Met-tRNAiMet binding to eukaryotic translation initiation factor eIF2. Nucleic Acids Res 47, 855-867.
Young-Baird, S.K., Lourenço, M.B., Elder, M.K., Klann, E., Liebau, S., Dever, T.E., 2020. Suppression of MEHMO Syndrome Mutation in eIF2 by Small Molecule ISRIB. Mol Cell 77, 875-886.e877.
Zubrienė, A., Matulienė, J., Baranauskienė, L., Jachno, J., Torresan, J., Michailovienė, V., Cimmperman, P., Matulis, D., 2009. Measurement of nanomolar dissociation constants by titration calorimetry and thermal shift assay - radicicol binding to Hsp90 and ethoxzolamide binding to CAII. Int J Mol Sci 10, 2662-2680.